Batteries

International Edition: DOI: 10.1002/anie.201511830
German Edition: DOI: 10.1002/ange.201511830

Functional Organosulfide Electrolyte Promotes an Alternate Reaction Pathway to Achieve High Performance in Lithium–Sulfur Batteries

*Shuru Chen, Fang Dai, Mikhail L. Gordin, Zhaoxin Yu, Yue Gao, Jiangxuan Song, and Donghai Wang**

Abstract: *Lithium–sulfur (Li-S) batteries have recently received great attention because they promise to provide energy density far beyond current lithium ion batteries. Typically, Li-S batteries operate by conversion of sulfur to reversibly form different soluble lithium polysulfide intermediates and insoluble lithium sulfides through multistep redox reactions. Herein, we report a functional electrolyte system incorporating dimethyl disulfide as a co-solvent that enables a new electrochemical reduction pathway for sulfur cathodes. This pathway uses soluble dimethyl polysulfides and lithium organosulfides as intermediates and products, which can boost cell capacity and lead to improved discharge–charge reversibility and cycling performance of sulfur cathodes. This electrolyte system can potentially enable Li-S batteries to achieve high energy density.*

The combination of lithium and sulfur is one of the most promising chemistries for the next generation of rechargeable lithium batteries owing to its high theoretical specific energy ($\approx$2600 Wh kg^{-1}) and potentially low cost.[1] Unlike intercalation-based lithium ion batteries, Li-S batteries operate by conversion of elemental sulfur to reversibly form lithium sulfide (Li_2S). This process involves the formation and multistep redox reactions of different soluble lithium polysulfide intermediates.[2] The dissolution of polysulfides in liquid electrolytes and the resulting "shuttle phenomenon" often lead to serious issues, such as active material loss, low Coulombic efficiency, and severe self-discharge, and has long been identified as one of the reasons for the poor cycle life of Li-S batteries.[3] The irreversible deposition of insoluble and insulating Li_2S on the cathode is known as another key reason for the rapid capacity fading.[4] Tremendous efforts have been made to address these issues, including the design of advanced carbon/sulfur (C/S) nanocomposites,[5] new cell configurations with polysulfide-blocking interlayers,[6] and more efficient electrolytes and additives.[7] Although these approaches have demonstrated improved performance by mitigating polysulfide dissolution and migration, none of them have fully addressed the key issues of Li-S batteries.

[*] Dr. S. Chen, Dr. F. Dai, Dr. M. L. Gordin, Z. Yu, Y. Gao, Dr. J. Song, Prof. D. Wang
Department of Mechanical and Nuclear Engineering
The Pennsylvania State University
University Park, PA 16802 (USA)
E-mail: dwang@psu.edu
Supporting information and the ORCID identification number(s) for the author(s) of this article can be found under: http://dx.doi.org/10.1002/anie.201511830.

Despite these issues, the dissolution of polysulfides actually plays a positive role in circumventing the insulating nature of sulfur species, helping Li-S cells to reach acceptable capacity and rate capability.[2b, 8] The dissolved polysulfides can be progressively reduced or oxidized on a conductive surface owing to the easy access of Li^+ through diffusion in the liquid electrolyte. The equilibrium reactions between sulfur (or Li_2S) and polysulfides also help enable the continuous reduction of non-conductive bulk sulfur during discharging (or the oxidation of insoluble Li_2S upon charging, respectively).[9] In this regard, the dissolved lithium polysulfides have been used, as either a "catholyte" or a co-salt/electrolyte additive while still having a sulfur cathode, to enhance electrochemical performance superior to the conventional Li-S cell configuration.[10] However, owing to the limited solubility of lithium polysulfides in organic electrolytes, extra electrolyte volume is needed to dissolve a large amount of lithium polysulfides and reach a high capacity.[11] Moreover, the cell capacity can be significantly reduced at high polysulfide concentrations owing to the increase in electrolyte viscosity and resistance.[12]

Departing from the use of lithium polysulfides as a co-salt/additive in electrolytes, we herein report a functional electrolyte system using a liquid organosulfur compound, dimethyl disulfide (DMDS), as a co-solvent for Li-S batteries. The DMDS contains a S–S bond that can reversibly cleave/reform upon discharging/charging, and has a theoretical capacity of 570 mAh g^{-1} (Supporting Information, Table S1). Because organic solvents commonly account for around 90 wt% of the electrolyte, substituting electrochemically active DMDS in place of a large fraction of the inactive solvents can significantly enhance Li-S cell capacity and help achieve high energy density. More importantly, investigation of the DMDS-containing electrolyte system using in operando proton nuclear magnetic resonance (^{1}H NMR) and other techniques showed that DMDS enables a new electrochemical reduction pathway for sulfur cathodes by formation and subsequent reduction of soluble dimethyl polysulfide (DMPS) species to form lithium organosulfides and lithium sulfides. The DMPS and lithium organosulfides show significantly improved redox kinetics and better reversibility, thus enabling lower charge overpotential and more stable cycling performance of sulfur cathodes in the optimized DMDS-containing electrolyte than that of Li-S cells using conventional electrolytes.

We first studied and compared the electrochemical performance of C/S cathodes in conventional ether-based electrolytes and electrolytes with varied DMDS contents. All of the coin cells tested contained $\approx$1 mg of sulfur and 10 μL of

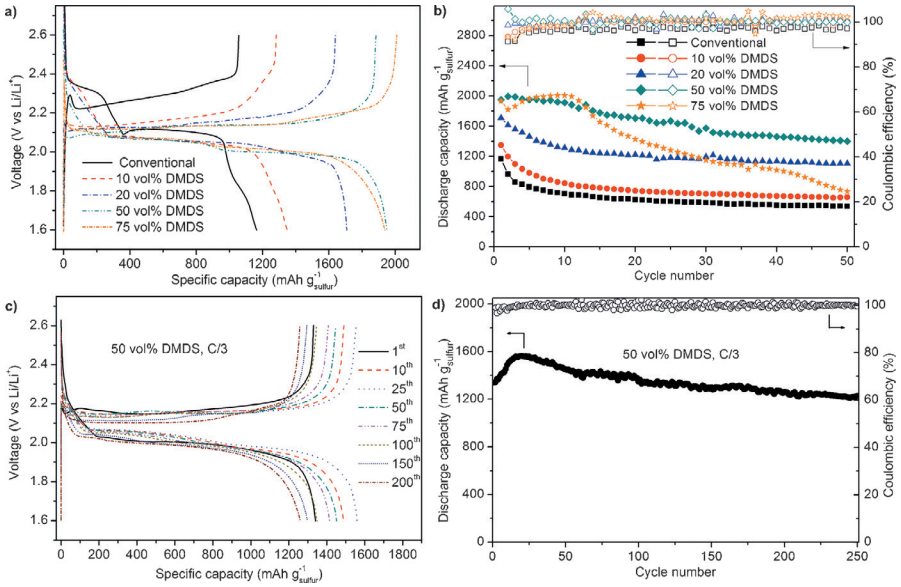

Figure 1. a) Initial discharge–charge profiles and b) cycling performance of C/S cathodes at C/10 rate in conventional and 10–75 vol% DMDS-containing electrolytes. c) Discharge–charge profiles and d) extended cycling performance of a C/S cathode in 50 vol% DMDS-containing electrolyte at C/3 rate. The specific capacities are calculated based on the mass of sulfur in the C/S cathodes.

electrolyte, resulting in an electrolyte/sulfur ratio of $\approx 10\,mL\,g^{-1}$ (Supporting Information), similar to the suggested optimal value in the literature.[13] As shown in Figure 1a, the C/S cathode in conventional electrolyte shows an initial sulfur-specific discharge capacity of $1164\,mAh\,g^{-1}$ with two typical discharge plateaus at 2.4–2.3 V and ≈ 2.1 V, corresponding to the reduction of solid S_8 to soluble polysulfides, and polysulfides to insoluble sulfides, respectively. In comparison, using the same amount of DMDS-containing electrolytes, the initial sulfur-specific discharge capacities of the C/S cathode increase to 1348, 1708, and $1950\,mAh\,g^{-1}$ with DMDS contents of 10, 20, and 50 vol%, respectively. The enhanced capacity can also be illustrated in terms of specific capacity based on the whole mass of the cathode and electrolyte, demonstrating the advantage of DMDS-containing electrolytes to boost the overall cell capacity (Figure S1). Besides the change in capacities, the high voltage discharge plateau at 2.4–2.3 V (in conventional electrolyte) disappears with increasing DMDS content and two different discharge plateaus at ≈ 2.05 and ≈ 2.0 V are observed. Furthermore, the charge plateau remarkably decreases from 2.2–2.4 V to 2.1–2.2 V, resulting in a much lower hysteresis between charge and discharge. The changes are consistent over cycling (Figure S2) and in line with cyclic voltammetry (CV) results (Figure S3), which show similar changes in redox peak structure and position. Increasing of DMDS content to 75 vol% does not further improve the capacity and leads to poor cycle life, probably owing to its low conductivity (Figure S4) and fast depletion of solvents.

Figure 1b shows that the C/S cathode has the optimized cycling performance with 50 vol% DMDS at C/10, reaching a maximum discharge capacity of $\approx 2{,}000\,mAh\,g^{-1}$ in the first few cycles. The sulfur-specific capacity remains $\approx 1{,}400\,mAh\,g^{-1}$ after 50 cycles, which is more than double the stable capacity of $\approx 600\,mAh\,g^{-1}$ with the conventional electrolyte. Rate capabilities of the C/S cathode in conventional electrolyte and electrolytes with varied DMDS contents were evaluated (Figure S5). Similarly, the optimal rate performance was also obtained with 50 vol% DMDS. Extended cycling (250 cycles) in the 50 vol% DMDS-containing electrolyte at a higher C/3 rate was also conducted, demonstrating the stable voltage profiles (Figure 1c) and excellent retention of discharge capacity (Figure 1d, $> 1{,}200\,mAh\,g^{-1}$) over longer cycling periods.

Based on the above results, it is clear that the use of DMDS-containing electrolytes can significantly boost cell capacity. Interestingly, the ≈ 1.9 V discharge plateau corresponding to direct reduction of DMDS (Figure S6) was not observed in Figure 1a for the cells using DMDS-containing electrolytes. This indicates a different discharge–charge mechanism of both sulfur and DMDS in this system, distinct from the superposition of the redox reactions of sulfur and DMDS. The smaller gap between discharge and charge curves and the remarkable cycling performance indicate that this mechanism has faster redox kinetics and better discharge–charge reversibility than that in the conventional electrolyte.

Previous research has shown that DMDS is capable of quickly dissolving sulfur by forming an equilibrated mixture of soluble dimethyl polysulfides (DMPS, $CH_3SS_mSCH_3$),[14] as confirmed by ^{1}H NMR results (Figure S7). The generated DMPS and its reduction could be responsible for the observed differences in electrochemical performances shown in Figure 1. To investigate the reaction mechanism, we assembled two transparent flask cells using conventional and 50 vol% DMDS-containing electrolytes. Similar differences to those seen in coin cells, in terms of capacities and discharge curves between the two electrolytes, were observed in the transparent cells (Figure 2a). This suggests similar discharge mechanisms in both coin cells and flask cells, even though the flask cells are flooded with electrolytes.

To elucidate the formation and subsequent reduction of new DMPS intermediates, in operando ^{1}H NMR studies of the electrolytes at various depths of discharge were conducted and photos were also taken during the initial discharge process. Because lithium polysulfides are ^{1}H NMR silent, only constant peaks from DOL and DME were observed in the conventional electrolyte (Figure S8). In addition to those peaks, the DMDS-containing electrolyte showed a significant increase in dimethyl trisulfide (DMTS, $\delta = 2.48$ ppm) at the early stages of discharge and the formation of a small amount of dimethyl tetrasulfide (DMTtS, $\delta = 2.57$ ppm), which are characteristic of the sulfur-DMDS reaction (Figure 2b).[14c]

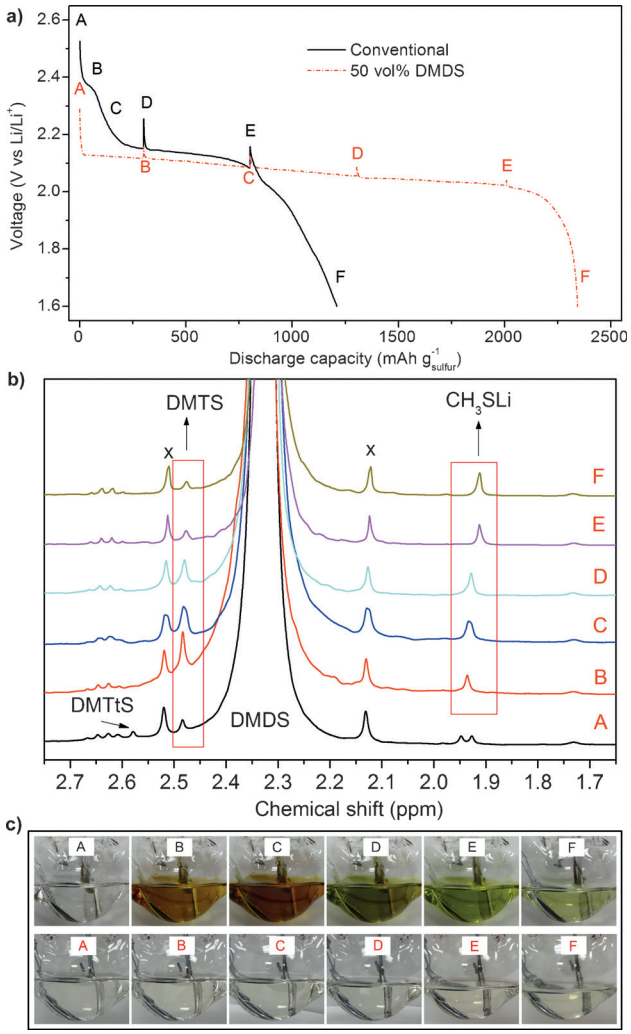

Figure 2. a) Initial discharge profiles of the flask cells with conventional (black) and 50 vol% DMDS-containing (red) electrolyte. b) ^{1}H NMR spectra of the DMDS-containing electrolyte at varying depths of discharge, corresponding to points marked in (a). The two peaks marked with *x* are satellites attributable to C^{13} coupling in DMDS. c) Photos showing the electrolyte color changes of both electrolytes at corresponding points in (a) during discharge.

Upon further discharging, the peak of DMTtS quickly disappeared while that of DMTS gradually decreased owing to their electrochemical reduction, which corresponds to the discharge plateaus between ≈2.0 and 2.1 V. The appearance of a new singlet peak at 1.93 ppm corresponding to CH_3SLi (Figure S9) was also noted; this peak grew initially then reached its maximum size when the discharge capacity rose above 800 mAh g^{-1}, probably due to the limited solubility of CH_3SLi. This could explain why DMDS itself is not directly reduced: the precipitation of CH_3SLi may passivate the conductive surface, cutting off the discharge process before the remaining DMDS in the electrolyte can be reduced. Therefore, only the DMDS that reacts with sulfur to form DMPS, which is more reactive than DMDS, is involved in the electrochemical reduction reactions and contributes capacity. Other possible reduction products are Li_2S_2/Li_2S (insoluble and ^{1}H NMR silent) and CH_3SSLi. However, the ^{1}H NMR peak of CH_3SSLi may overlap with the broad peak of DMDS and cannot be directly observed in these spectra.

In operando ^{1}H NMR studies of the 50 vol% DMDS-containing electrolyte at various depths of both discharge and charge processes were also conducted. Regeneration of DMTS and disappearance of CH_3SLi upon charging were observed (Figure S10), which indicate the reversibility of the DMDS-containing electrolyte system and further confirm the new reaction mechanism, as summarized below.

$$CH_3SSCH_3 + \frac{m}{8}S_8 \leftrightarrow CH_3SS_mSCH_3 \quad (1)$$

$$CH_3SS_mSCH_3 + 2(m+1)Li^+ + 2(m+1)e^- \leftrightarrow 2\,CH_3SLi + mLi_2S \quad (2)$$

The $CH_3SS_mSCH_3$ represents a mixture with *m* mainly equalling 1 and 2 based on the above NMR results.

In addition to the NMR results, obvious differences in the colors of the two electrolytes during the discharge process are observed (Figure 2c). Upon discharging, the conventional electrolyte changes from clear to dark red, then to green, and finally to light yellow due to the presence of lithium polysulfides with different sulfur chain lengths and concentrations.[15] The DMDS-containing electrolyte changes very little at early discharge steps (point A to D in Figure 2c) and then to a slightly cloudy and straw-colored liquid at the end of discharge (point E to F in Figure 2c), indicating the absence of lithium polysulfides and further confirming the new reaction pathway by the formation of DMPS intermediates and lithium organosulfides.

To identify the discharge products, C/S cathodes and sulfur-free carbon electrodes discharged in coin cells with both conventional and 50 vol% DMDS-containing electrolytes were investigated using scanning electron microscopy (SEM), X-ray diffraction (XRD), and X-ray photoelectron spectroscopy (XPS). Morphological and structural differences in the solid discharge products with different electrolyte systems were found from the SEM and XRD results (Figure S11). Consistent with previous results, broad XRD peaks from aggregated sub-micron-sized Li_2S particles were clearly observed after discharging the C/S cathode in conventional electrolyte.[16] The sulfur-free electrode discharged in the DMDS-containing electrolyte instead showed very large particles (diameter of ≈100 μm) with intense XRD peaks, which can be ascribed to highly crystalline CH_3SLi, the only reduction product of DMDS. In contrast, the C/S cathode discharged in DMDS-containing electrolyte was covered by numerous plate-like particles around 10–50 μm in size, along with aggregated sub-micron-sized particles, and showed major XRD peaks from both Li_2S and CH_3SLi, indicating the existence of both products.

The solid discharge products were further identified by XPS (Figure 3). The XPS spectrum of the as-prepared C/S cathode was obtained as an additional reference, and exhibited a pair of characteristic S $2p_{3/2}$ and S $2p_{1/2}$ peaks of neutral sulfur at 164.0 eV and 165.2 eV.[17] In agreement with the literature data,[18] the XPS spectrum of the C/S cathode discharged in conventional electrolyte showed three pairs of S $2p_{3/2}$ and S $2p_{1/2}$ dual peaks, which are evidence of three sulfur

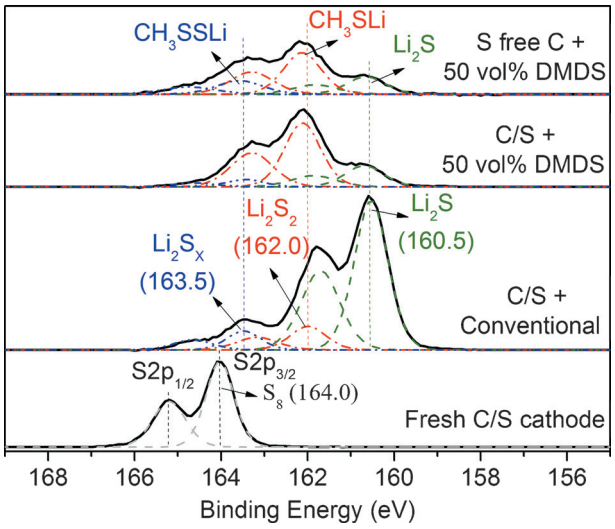

Figure 3. S_{2p} XPS spectra of a fresh C/S cathode, sulfur-free carbon cathode discharged in 50 vol% DMDS-containing electrolyte, and C/S cathode discharged in both conventional and 50 vol% DMDS-containing electrolytes.

species: primarily Li_2S (S $2p_{3/2}$ at 160.5 eV) along with smaller amounts of Li_2S_2 (S $2p_{3/2}$ at 162.0 eV) and polysulfides (S $2p_{3/2}$ at 163.5 eV). In the sulfur-free electrode discharged with the DMDS-containing electrolyte, a major XPS peak was observed at 162.0 eV (a similar position to that of Li_2S_2), which is ascribed to the S $2p_{3/2}$ for CH_3SLi, the reduction product of DMDS. Smaller peaks at ≈160.5 and ≈163.5 eV were also observed, corresponding to small amounts of Li_2S and CH_3SSLi, respectively. They probably come from the reduction of the DMTS impurity in the DMDS (the presence of which was seen in the NMR spectra in Figure S7). When discharging the C/S electrode in DMDS-containing electrolyte, the spectrum appears similar to that of the sulfur-free electrode, with a relatively stronger peak of CH_3SLi at 162.0 eV. Additionally, the relative intensity of the Li_2S peak was much weaker than that observed in the conventional electrolyte system, indicating the formation of less Li_2S at the end of discharge. It was further confirmed that the discharge process shuts off mainly due to the surface passivation by CH_3SLi and some other lithium organopolysulfide (e.g., CH_3SSLi) products, rather than by Li_2S as in conventional electrolytes. As indicated by the lower charge overpotential (Figure 1a) and the CV profile (Figure S3), these discharge products also showed better kinetics and reversibility upon charging than insoluble Li_2S in conventional electrolyte, which can be beneficial to the cycling performance.

In conclusion, we reported a functional electrolyte system using DMDS as a co-solvent for Li-S batteries. DMDS was found to react with sulfur to form soluble methyl-terminated polysulfide intermediates, which are further reduced to lithium organosulfides during the discharge process. Through this new mechanism, the DMDS-containing electrolyte not only contributes extra capacity to the cell, reaching almost double the value obtained in the conventional Li-S electrolyte, but also enables robust performance of sulfur cathodes. This work thus provides a strategy for improving the practical energy density of Li-S batteries. However, it is worth noting that the soluble organopolysulfides and DMDS can still corrode the lithium anode and cause shuttle effects and self-discharge issues (Figure S12) similar to lithium polysulfides. Thus, $LiNO_3$ is still needed to protect the lithium anode and improve the charge efficiency. This indicates the continued need for development of anode protection technology to couple with this electrolyte system and meet the demands of practical applications.

Acknowledgements

This work was supported by the Assistant Secretary for Energy Efficiency and Renewable Energy, Office of Vehicle Technologies of the U.S. Department of Energy under Contract No. DEEE0005475. We thank Dr. Wenbin Luo from Department of Chemistry at the Pennsylvania State University for her help with NMR measurement. We also thank Dr. Vincent Bojan and Dr. Greg Barber at the Pennsylvania State University for their help with air-sensitive XPS characterization and analyses.

Keywords: batteries · dimethyl disulfide · electrolytes · lithium–sulfur · organosulfides

How to cite: *Angew. Chem. Int. Ed.* **2016**, *55*, 4231–4235
Angew. Chem. **2016**, *128*, 4303–4307

[1] a) P. G. Bruce, S. A. Freunberger, L. J. Hardwick, J. M. Tarascon, *Nat. Mater.* **2012**, *11*, 19–29; b) S. Urbonaite, T. Poux, P. Novák, *Adv. Energy Mater.* **2015**, *5*, 1500118.
[2] a) R. D. Rauh, K. M. Abraham, G. F. Pearson, J. K. Surprenant, S. B. Brummer, *J. Electrochem. Soc.* **1979**, *126*, 523–527; b) H. Yamin, A. Gorenshtain, J. Penciner, Y. Sternberg, E. Peled, *J. Electrochem. Soc.* **1988**, *135*, 1045–1048; c) K. Kumaresan, Y. Mikhaylik, R. E. White, *J. Electrochem. Soc.* **2008**, *155*, A576–A582.
[3] S. S. Zhang, *J. Power Sources* **2013**, *231*, 153–162.
[4] C. Barchasz, J. C. Lepretre, F. Alloin, S. Patoux, *J. Power Sources* **2012**, *199*, 322–330.
[5] a) S. Xin, L. Gu, N. H. Zhao, Y. X. Yin, L. J. Zhou, Y. G. Guo, L. J. Wan, *J. Am. Chem. Soc.* **2012**, *134*, 18510–18513; b) B. Zhang, X. Qin, G. R. Li, X. P. Gao, *Energy Environ. Sci.* **2010**, *3*, 1531–1537; c) X. L. Ji, K. T. Lee, L. F. Nazar, *Nat. Mater.* **2009**, *8*, 500–506; d) S. R. Chen, Y. P. Zhai, G. L. Xu, Y. X. Jiang, D. Y. Zhao, J. T. Li, L. Huang, S. G. Sun, *Electrochim. Acta* **2011**, *56*, 9549–9555; e) N. Jayaprakash, J. Shen, S. S. Moganty, A. Corona, L. A. Archer, *Angew. Chem. Int. Ed.* **2011**, *50*, 5904–5908; *Angew. Chem.* **2011**, *123*, 6026–6030; f) T. Xu, J. Song, M. L. Gordin, H. Sohn, Z. Yu, S. Chen, D. Wang, *ACS Appl. Mater. Interfaces* **2013**, *5*, 11355–11362; g) J. Song, T. Xu, M. L. Gordin, P. Zhu, D. Lv, Y.-B. Jiang, Y. Chen, Y. Duan, D. Wang, *Adv. Funct. Mater.* **2014**, *24*, 1243–1250; h) J. Song, M. L. Gordin, T. Xu, S. Chen, Z. Yu, H. Sohn, J. Lu, Y. Ren, Y. Duan, D. Wang, *Angew. Chem. Int. Ed.* **2015**, *54*, 4325–4329; *Angew. Chem.* **2015**, *127*, 4399–4403.
[6] a) Y. S. Su, A. Manthiram, *Nat. Commun.* **2012**, *3*, 1166; b) J. Song, Z. Yu, T. Xu, S. Chen, H. Sohn, M. Regula, D. Wang, *J. Mater. Chem. A* **2014**, *2*, 8623–8627.
[7] a) M. Cuisinier, P. E. Cabelguen, B. D. Adams, A. Garsuch, M. Balasubramanian, L. F. Nazar, *Energy Environ. Sci.* **2014**, *7*, 2697–2705; b) N. Azimi, W. Weng, C. Takoudis, Z. Zhang,

Electrochem. Commun. **2013**, *37*, 96 – 99; c) M. L. Gordin, F. Dai, S. Chen, T. Xu, J. Song, D. Tang, N. Azimi, Z. Zhang, D. Wang, *ACS Appl. Mater. Interfaces* **2014**, *6*, 8006 – 8010; d) Z. Lin, Z. C. Liu, W. J. Fu, N. J. Dudney, C. D. Liang, *Adv. Funct. Mater.* **2013**, *23*, 1064 – 1069; e) Y. V. Mikhailik, **2008**, U.S. Patent 7,553,590; f) D. Aurbach, E. Pollak, R. Elazari, G. Salitra, C. S. Kelley, J. Affinito, *J. Electrochem. Soc.* **2009**, *156*, A694 – A702.

[8] a) H. Yamin, E. Peled, *J. Power Sources* **1983**, *9*, 281 – 287; b) E. Peled, Y. Sternberg, A. Gorenshtein, Y. Lavi, *J. Electrochem. Soc.* **1989**, *136*, 1621 – 1625.

[9] a) Y. Yang, G. Zheng, S. Misra, J. Nelson, M. F. Toney, Y. Cui, *J. Am. Chem. Soc.* **2012**, *134*, 15387 – 15394; b) S. S. Zhang, *Electrochim. Acta* **2012**, *70*, 344 – 348.

[10] a) L. M. Suo, Y. S. Hu, H. Li, M. Armand, L. Q. Chen, *Nat. Commun.* **2013**, *4*, 1481; b) S. Chen, F. Dai, M. L. Gordin, D. Wang, *RSC Adv.* **2013**, *3*, 3540 – 3543; c) R. Xu, I. Belharouak, J. C. M. Li, X. Zhang, I. Bloom, J. Bareño, *Adv. Energy Mater.* **2013**, *3*, 833 – 838; d) R. Demir-Cakan, M. Morcrette, Gangulibabu, A. Guéguen, R. Dedryvère, J.-M. Tarascon, *Energy Environ. Sci.* **2013**, *6*, 176 – 182; e) S. S. Zhang, J. A. Read, *J. Power Sources* **2012**, *200*, 77 – 82; f) X. Yu, Z. Bi, F. Zhao, A. Manthiram, *ACS Appl. Mater. Interfaces* **2015**, *7*, 16625 – 16631.

[11] S. S. Zhang, D. T. Tran, *J. Power Sources* **2012**, *211*, 169 – 172.

[12] M. Hagen, P. Fanz, J. Tübke, *J. Power Sources* **2014**, *264*, 30 – 34.

[13] S. S. Zhang, *Energies* **2012**, *5*, 5190 – 5197.

[14] a) P. D. Clark, E. Fitzpatrick, C. S. C. Lau, C. O. Oriakhi, *Energy Fuels* **1993**, *7*, 155 – 158; b) S. Yamada, D. H. Wang, S. R. Li, M. Nishikawa, E. W. H. Qian, A. Ishihara, T. Kabe, *Chem. Commun.* **2003**, 842 – 843; c) D. Grant, J. R. Vanwazer, *J. Am. Chem. Soc.* **1964**, *86*, 3012 – 3017; d) P. D. Clark, C. O. Oriakhi, *Energy Fuels* **1992**, *6*, 474 – 477.

[15] Y. J. Li, H. Zhan, S. Q. Liu, K. L. Huang, Y. H. Zhou, *J. Power Sources* **2010**, *195*, 2945 – 2949.

[16] a) N. A. Cañas, S. Wolf, N. Wagner, K. A. Friedrich, *J. Power Sources* **2013**, *226*, 313 – 319; b) S. Cheon, S. Choi, J. Han, Y. Choi, B. Jung, H. Lim, *J. Electrochem. Soc.* **2004**, *151*, A2067 – A2073.

[17] M. Helen, M. A. Reddy, T. Diemant, U. Golla-Schindler, R. J. Behm, U. Kaiser, M. Fichtner, *Sci. Rep.* **2015**, *5*, 12146.

[18] Y. Fu, C. Zu, A. Manthiram, *J. Am. Chem. Soc.* **2013**, *135*, 18044 – 18047.

Received: December 21, 2015
Revised: January 28, 2016
Published online: February 25, 2016

